Ninth International Conference on CFD in the Minerals and Process Industries
CSIRO, Melbourne, Australia
10-12 December 2012

NUMERICAL INVESTIGATION OF BUBBLE INDUCED ELECTRICAL RESISTANCE IN ALUMINIUM REDUCTION CELLS

Kaiyu ZHANG[1,3], Yuqing FENG[1*], Peter WITT[1], William YANG[2], Mark COOKSEY[2], Zhaowen WANG[3] and M. Phil SCHWARZ[1]

[1] CSIRO Mathematics, Informatics and Statistics, Clayton, Victoria 3169, AUSTRALIA
[1] CSIRO Process Science and Engineering, Clayton, Victoria 3169, AUSTRALIA
[3] School of Metallurgical Engineering, Northeastern University, Shenyang, CHINA
*Corresponding author, E-mail address: Yuqing.Feng@csiro.au

ABSTRACT

A gas layer in the form of bubbles exists at the bottom surface of anodes in aluminium electrolytic cells in the Hall-Heroult process. The gas bubbles increase electrical resistance, cause an additional voltage drop and increase energy consumption. While the presence of gas bubbles is an inherent feature of the process, it is important to assess their contribution to voltage drop however this is difficult to study in detail experimentally.

This paper presents a quantitative assessment of the bubble induced electrical resistance using a computational fluid dynamics (CFD) modelling platform. Using two-dimensional geometry of part of an electrolytic cell as test bed, the current flow was simulated with the presence of a bubble layer beneath the anode. Detailed information on the bubble layer was obtained from an air-water model using a digital camera to capture the transient bubbling dynamics. The simulations were conducted at different gas generation rates representing different current densities.

The simulated bubble induced voltages are within the range of the experimental measurement results on commercial cells from other researchers. Predicted bubble resistances are within the range of published empirical correlations, but do not fit in any particular expression. The presence of bubbles does not greatly affect global current flow in the whole cell, but it does significantly affect the local current flow at the anode bath interface. Local peaks in current flow occur at the bubble and liquid boundary on the anode.

INTRODUCTION

The Hall-Héroult process is the only process at the industrial scale for producing aluminium from alumina. The process uses a huge amount of electricity, approximately 13 kilowatt hours (kWh) of electrical energy to produce one kilogram of aluminium, of which, only about 50% is used to decompose alumina into aluminium, and the rest is generated as waste heat. There is pressure on the aluminium smelting industry to reduce energy consumption for both cost and environmental considerations.

A significant contribution to the waste energy, or cell voltage, is from CO_2 gas bubbles produced on the underside of the carbon anode. The contribution of bubbles to voltage drop is in the order of 0.25 V from a total cell voltage of 4.0-4.6 V. As shown in a recent review paper (Cooksey et al., 2008), the bubble induced electrical resistance has been extensively studied in industrial cells, laboratory cells and physical models. However, despite being an intensive research topic, the detailed contribution of bubbles to voltage drop is not fully understood due to the complex of the bubble dynamics, e.g. bubble size, bubble layer thickness and the variation in cell voltage. The empirical equations to predict bubble induced resistance vary significantly (Cooksey et al., 2008).

Numerical models can simulate the detailed current flow around individual bubbles and thus provide an excellent opportunity to quantitatively assess the bubble induced voltage drop. Nowadays, numerical techniques have been developed to study various aspects of the aluminium smelting process, such as electro-magnetic models to improve bus-bar design, thermal-electric models to improve electrical connection (Molenaar and Ding, 2011) and computational fluid dynamics (CFD) models to investigate bubble induced flow, alumina mixing and individual bubble behaviour (Feng et. al, 2011). There is very limited numerical work (Einarsrud et. al, 2011) that investigates the electrical resistance and detailed current flow with the presence of bubbles under the anode.

This paper presents a study in this direction. Using a two-dimensional (2D) geometry of part of a real cell as the testing bed, current flow in the domain is calculated using ANSYS/Fluent as the numerical platform. The bubble induced voltage drop is quantified through simulations with and without the presence of bubbles in anode to cathode distance (ACD). Investigations were conducted for different bubble coverage areas so as to account for different current densities.

Simulation results are compared with various empirical correlations to check their relative relevance. For the first time, the current distribution around bubbles is investigated in detail.

MODELLING METHOD

Modelling Methodology

To realistically model the voltage drop due to bubbles, details of bubble profile and coverage on the anode is required. Bubble dynamics can be obtained through physical modelling using advanced measurement techniques or numerical modelling using surface capturing methods (Zhang et al., 2012). Recently, the bubbling dynamics in an aluminium smelting environment has been studied numerically (Subrat et al., 2011; Einarsrud, 2010; and Zhang

et al., 2012), but to fully capture the detailed bubble dynamics is proving to be a non-trivial effort with current computing facilities. In this study, an air-water physical model is used to obtain detailed bubble morphology. This bubble information is then used to set up a numerical model.

Physical Modelling

Figure 1 shows the main features of the air-water model used to obtain bubble morphology information. The model consists of a transparent Plexiglas container (890mmx100mmx290mm) with a suspending box-shaped Plexiglas "anode" (650mmx100 mmx240 mm high), which fits tightly between the walls of the container. The anode box was subdivided into two equal air-tight compartments.

Air flow rate into each compartment is individually controlled to ensure a uniform gas distribution over the anode face. The distance between the anode and the bottom of the container could be adjusted. The formation of bubbles in an aluminium reduction cell is very complex and the detailed bubble formation mechanism is still not very clear. In the present research, gas evolution was simulated by passing compressed air through a micro-porous high density polyethylene plate that modelled the anode's bottom surface. The cell was fixed on a steel table with a glass tabletop and adjustable table leg; this permitted the entire cell to be tilted. In the current experiment, the tilt angle was set as 1.5 degree along the direction of the long edge of the anode slices (as might occur because of anode consumption), the ACD is set to 50 mm and the bath depth used was 150mm.

Changes in cell current are accounted for by varying the air flow rate through the porous polyethylene plate. In an operating cell increased current increases reduction of alumina and increases production of CO_2 bubbles. Because the present physical model only represents a narrow transverse slice of a prebake cell, the ability for bubbles escaping in the third dimension is lost. Therefore, the air injection rate applied in this work (4L/min and 8L/min) approximately correspond to a current density in the range of 0.6 ~ 1.5A/cm^2.

Measurements were performed by a high resolution digital camera that is set right underneath the anode to capture images of the bubble morphology in ACD. The direction of the camera was adjusted to capture the best images of bubble morphology. Recordings for each experimental condition were made at two locations since the camera lens field of view was not large enough to catch the whole underside of the anode plate.

Numerical Modelling

Electrical current flow can be simulated by using different modelling methods and numerical platforms, such as finite element analysis (FEA) modelling in Abaqus and finite control volume method in CFD modelling (ANSYS CFX and Fluent). The FEA model treats every part as a solid, but it is not possible to simulate the dynamic motion of bubbles planned for future work. The ANSYS/Fluent software has been used in the past to study bubble dynamics (Zhang et al., 2012), and has the potential for fully coupling bubble flow and current flow in future work, and is therefore, selected for this study.

For a fast analysis, the study is conducted using a two-dimensional (2D) geometry. Figure 2 shows the 2D geometry used in the simulation. The geometry represents a slice of a typical commercial Hall–Héroult prebake cell, but is not related to any specific cell design. The bath domain is the same size as the physical model. To reasonably represent a real aluminium smelting process, the parts included in the model are: anode, liquid bath, metal, cathode and collect bar (Figure 2). Current flows in from the top of the anode and flows out from the end of the collect bar, thus these two faces are set as an inlet and outlet for the current, respectively. All the other boundaries are set as insulation boundaries. The input current density is 0.7 A/cm^2.

To calculate additional electrical resistance induced by the presence of the bubbles underneath the anode, the Laplace equation

$$\nabla^2 V = 0$$

is solved within the domain shown in Figure 2 with bubble layer obtained from the experiments. V represents electrical potential, or voltage (v);

In current numerical modelling, the transient VOF model is used. Even though the Navier-Stokes equations are solved, and bubble dynamics can be obtained but because present work focus on the current flow under specific bubble distribution captured in physical modelling, so the calculation only processed with in one small time step (10^{-50}s). Further work with continuous gas injection of gases is needed to better represent the aluminium smelting process and to quantify the fluctuations in voltage drop and current distribution variation.

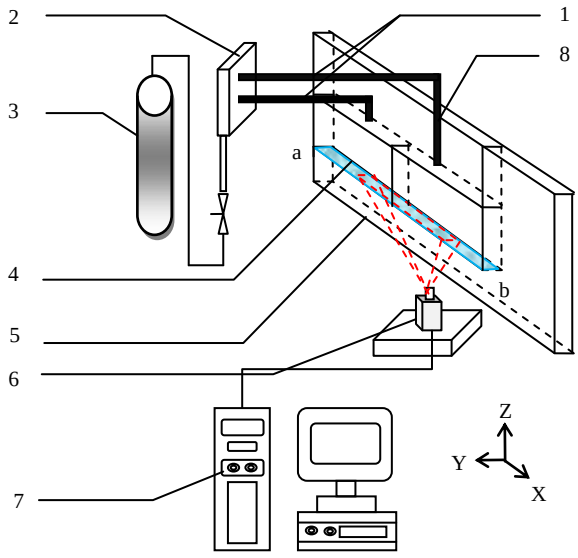

1. Pipe 2.Bubble injector regulator panel 3.Air cylinder
4. Porous panel 5. Transparent water sink 6. Camera
7. Computer 8. Anode zone
Side a : The centre of the anode Side b: The edge of the anode

Figure 1: Schematic diagram of air-water model setup and bubble measurement arrangement

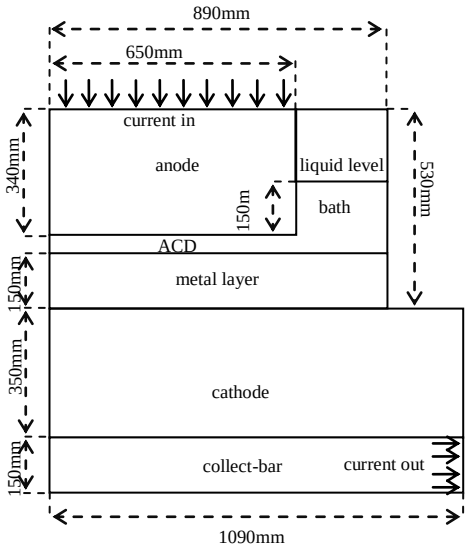

Figure 2: Two-dimensional numerical simulation domain

In setting up the model the following simplifications are made:

- The bubble information in the side channels is not included due to the difficulty of measurement and it only having a small effect on current flow;
- The effect of temperature on the electric conductivity is not considered. As shown in Table 1, a fixed value is set for each lining materials and liquid metal. The effect of alumina concentration on bath electric conductivity is not considered either;
- The model is setup at for a number of different time instants to give information on different bubble states. The liquid motion on current flow is neglected, hence assuming that the voltage is the dominant factor in determining current flow.

Table 1: Electrical conductivity for different materials

Material	Conductivity [S m^{-1}]
Anode	$2.143x10^{4}$
Cathode	$5.000x10^{4}$
Gas	$9.85x10^{-6}$
Cryolite	$2.220x10^{2}$
Steel	$7.587x10^{5}$
Metal	$4.167x10^{5}$

In present work, a commercial CFD package (ANSYS-Fluent) based on the Finite Volume Method was used as the numerical modelling tool. The mesh is refined at the interface of the bubble and around the underside of the surface, allowing more accurate capturing of the detailed current flow paths around the bubbles. The maximum cell surface area is set as $5x10^{-6}$ m^2 and the minimal cell surface area is set as $6.0x10^{-9}$ m^2. The absolute convergence criteria for continuity and velocity are both set as 10^{-7}.

RESULTS AND DISCUSSION

Bubble Measurement in ACD

Figure 3 plots the bubble shape on the underside of the anode at three time instants for a gas flow rate of 4 L min^{-1} (Figure 3 A,B,C) and 8 L min^{-1} (Figure 3 D,E,F). Due to the different reflection of gas and liquid, bubble boundaries can be clearly captured by digital photographic camera, e.g. bubble region is brighter than the bubble free region.

Following the injection of air through the porous panel, small tiny bubbles start to appear randomly on the underside of the anode. These tiny bubbles start to grow with the continuous injection of gas. When a bubble's size is large enough, it starts to slide towards the high end of the anode due to the buoyancy effect. During the sliding process, the bubble absorbs the front bubbles to form a larger bubble. This bubble coalescence process results in much larger bubbles at the higher end of the anode (side b) than at the low end of the anode (side a). Fortin reported the same phenomenon and described it as a "sweeping effect" in his work: such that the bubbles gain size and speed during a typical coalescing process (Fortin et al., 1984).

The gray scale photographic images are converted to black and white images using the light intensity filter function in the Photoshop software. Thus, the bubble boundaries can be identified clearly. In the present model a two-dimensional geometry is used, bubble information at the centre of the anode width direction (red line in the Figure) is used as the bubble size in the model.

As the photo images only capture two dimensions of the bubbles, the bubble thickness cannot be obtained directly. From the experiment it is not straightforward to determine the bubble layer thickness or three-dimensional shape. Some simplification of the shape is made in the numerical model setup. The body of the bubble is assumed to be parallel with the anode base and the head and tail are assumed to be of a constant radius. Using a probe that transfers a signal when it occasionally contacts a gas bubble, Haupin (1971) found the gas bubble layer thickness under the margin of the anode in a real cell to be approximately 5mm. Accordingly, the bubble layer thickness in the model is set as 5 mm with the length varied to account for different bubble sizes. From visual observations the bubble layer thickness in the air-water model is of a similar value. It is reported that the contact angle of molten electrolyte on a graphite sample was measured around 120° (Grjotheim, 1982; Gassayre and Bouvet, 2002). Hence, the geometry of the head and tail is constructed to fit this angle. For bubbles with a diameter less than 5mm, the parallel region of the bubble was not constructed and bubble consisted of only the head and the tail. Following these simplification, the 2D bubble profile is sketched below each black white image.

Table 2 gives the statistics of the bubble information obtained from the experiments. Bubble coverage is about 40% at the lower gas flow rate of 4 L/min and is about 50% when the gas flow rate is doubled. The bubble coverage agrees reasonably well with the past experimental work (Aaberg et al. 1997). The bubble coverage varies with time, but remains within a range around 10%. Further statistical analysis based on the whole anode surface area will be performed to study the variation of the bubble coverage with time in detail.

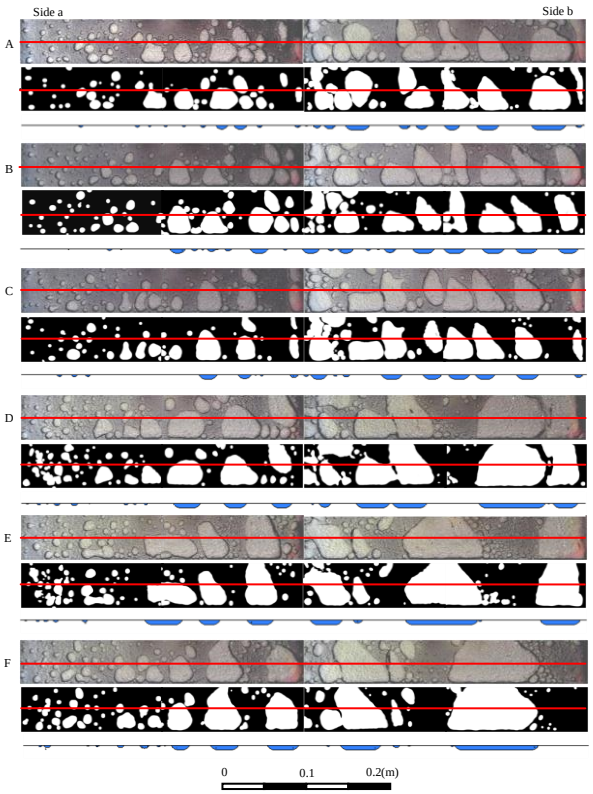

Figure 3: Snapshots of bubble morphology in ACD: A, B, C represent three instants when the gas flow rate is 4 L/min, and D, E, F represent three instants when the gas flow rate is 8 L/min. The bubble information at the red line is used for 2D numerical model setup.

Table 2: Measured bubble number and coverage beneath the anode used to set up the 2D model

Sample No.	Gas flow rate [l min^{-1}]	Number of bubbles	Anode Bubble coverage
A	4	20	37%
B	4	22	40%
C	4	18	36%
D	8	19	50%
E	8	13	47%
F	8	17	46%

Voltage Drop

Figure 4 shows the predicted voltage profile without the presence of a bubble layer in Figure 4(a) and with a bubble layer in Figure 4(b). Clearly, the presence of a bubble layer leads to a higher voltage drop across the cell. As shown by the contour map, the highest voltage gradient occurs in the bath region, indicating that most energy loss due to electrical resistance occurs in the bath.

Figure 5 shows the extra voltage drop due to the presence of bubbles. The data points correspond to the 6 instants shown in Figure 3. Generally, the voltage drop increases as the bubble coverage increases. Increasing the bubble coverage from 37% to 50% results in an increase of the extra voltage from 0.11 V to 0.29 V at this fixed current density (0.7A cm^{-2}). At a fixed gas flow rate (4 L min^{-1} or 8 L min^{-1}), the bubble coverage and the voltage drop fluctuates, which implies that bubble layer is a cause for voltage fluctuations in a real cell.

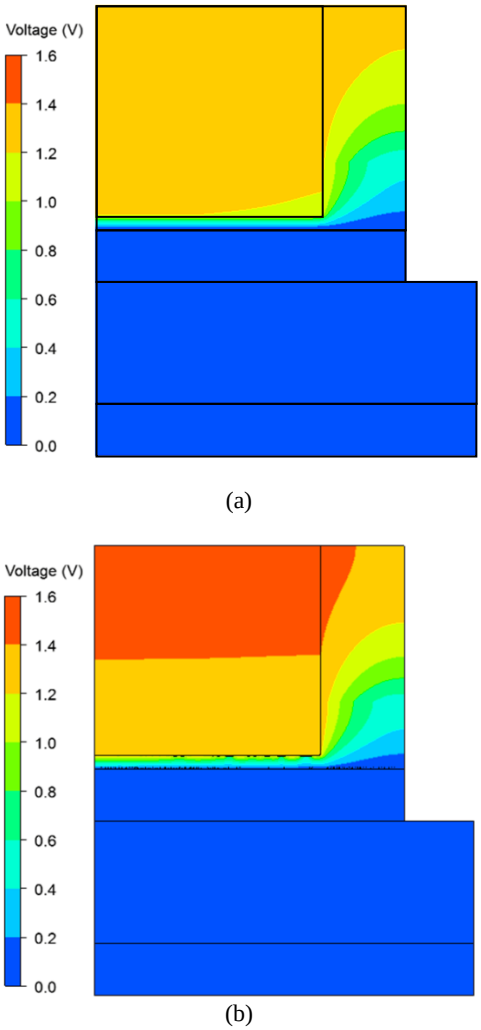

Figure 4: Voltage potential distribution: (a) without the presence of bubbles; (b) with the presence of bubbles for the case shown in Figure 3 A.

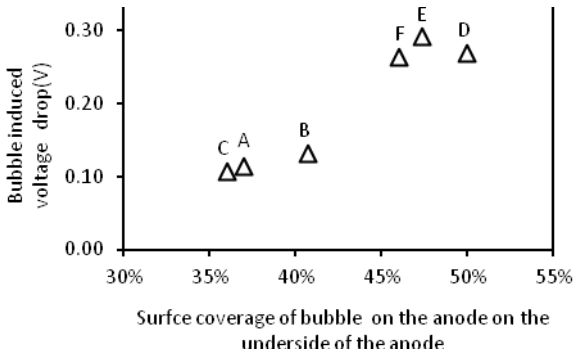

Figure 5: Bubble contributed voltage drop at different bubble surface coverage.

It is interesting to note that the highest bubble coverage does not lead to the highest voltage drop (Case D is lower than Case E). Table 2 shows that the number of bubbles in case D is much higher than in case E. Possibly the bubble size distribution contributes to this, further investigation in the future is needed to confirm this.

In the current simulation, the same total current is used for both gas generation rates. This might underestimate the contribution of gas coverage on voltage drop as high gas coverage is often related to high current density. Therefore, instead of comparing the value of voltage drop, it is more reasonable to compare the bubble induced resistance, which is commonly used in the literature. Table 3 summarises existing bubble resistance models derived from both experiment works and theoretical investigation. It can be observed that the predominant parameters used are bubble coverage fraction (f) and bubble layer thickness (d_b). Figure 6 compares the simulated bubble resistance with these different correlations.

Results from the computational model are in the range of the semi-empirical formula values, but do not fit any independent expression. The resistance predicted by the model when bubble coverage is lower are close to values from expression 1, but when the coverage is high, agree with values from expression 4. These results suggest that the growth rate of bubble resistance corresponding to the increase of bubble coverage is higher than given by any of the published expressions. Future three-dimensional simulations might be necessary to further clarify this.

Table 3 Published expressions for bubble induced electrical resistance

NO	Expression	Author
1	$\Delta R = k_0 \times d_b \times ((1/(1-f)-1)/A$	Cooksey et al., 2008
2	$\Delta R = k_0 \times d_b \times ((1+f/2)/(1-f)-1)/A$	Maxwell, 1954
3	$\Delta R = k_0 \times d_b \times 1.3524 \times f/A$	Sides et al., 1980
4	$\Delta R = k_0 \times d_b \times [(1-f)^{-1.5}-1]/A$	Solheim et al., 1986
5	$\Delta R = k_0 \times d_b \times ((1-\varepsilon_b)^{-1.5}-1)/A$	Thonstad, 2001

ΔR: the extra resistance due the existing bubble
k_0: the resistivity of the cryolite
d_b: the depth of the bubble layer
f: fractional surface coverage by bubbles
ε_b: volume fraction of bubbles in ACD
A: the area of the underside surface of anode

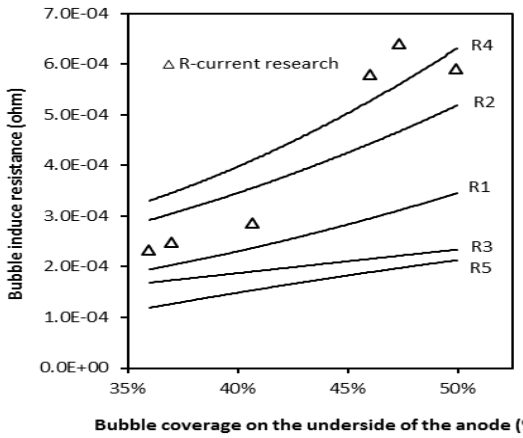

Figure 6: Bubble resistance at different bubble coverage.

Current Flow

The influence of bubbles is further investigated by plotting the current flow distribution. Figure 7(a) plots the current flow in the full simulation domain without the presence of a gas bubble layer. The current flow is almost uniformly downward in the anode and ACD, with only a small current in the side channel. In the metal layer, a strong horizontal component to the current flows is predicted. This is probably, due to the high conductivity of the metal layer, and low voltage potential on the side of the collector bar. When the current passes through the cathode, it changes its direction to the horizontal direction and flows out through the end of the collector bar. When a bubble layer is present (Figure 8a, corresponding the case of Figure 3A), the overall current flow is similar to the case without the presence of a bubble layer (Figure 7a). This implies that the presence of a bubble layer does not make a significant change to current flow in the cell.

Figure 7b and Figure 8b show a close-up view of current flow at the anode-bath interface without and with the presence of a bubble layer respectively. Without the bubble layer (Figure 7b), the current flow is quite uniform. When a bubble layer is present, increased resistance from the gas layer prevents current directly passing through the bubble. Current in the anode above the bubble changes its direction and flows through gaps between the bubbles. Consequently, a high local concentration of current density occurs at the contacting point at the intersection of the anode, gas and bath.. It is easy to understand that bubbles reduce the area for current flow thereby increasing the resistance and local current hence leading to an extra voltage drop which is regarded as the bubble induced voltage drop. Therefore, the bubble induced voltage drop is closely related to bubble coverage area and gas layer thickness which is quite consistent with those exiting bubble resistance expressions listed in Table 2.

The detailed current flow predictions show that current is not uniform near the bubbles. This indicates that the Lorentz force, which is a function of current density, at the gas-bath interface of bubble likely to also be non-uniform, and may substantially affect bubble motion. In the current model neither bubble dynamics nor the Lorentz force are included. In future work it is worthwhile to investigate the effect this change in current density has on bubble motion.

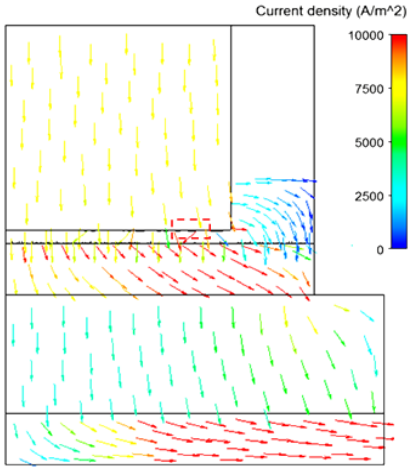

(a)

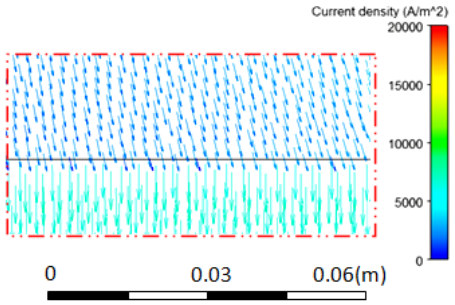

(b)

Figure 7: Current flow without the bubble layer: (a) full simulation domain; (b) a close-up view near the anode-bath interface.

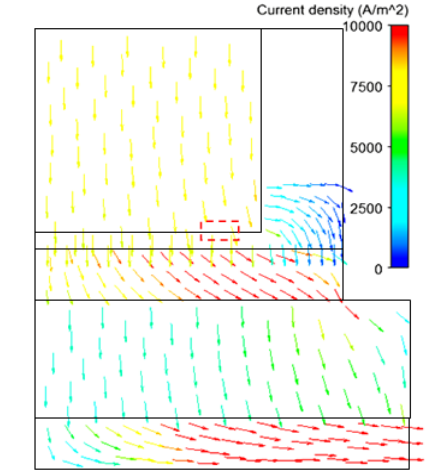

(a)

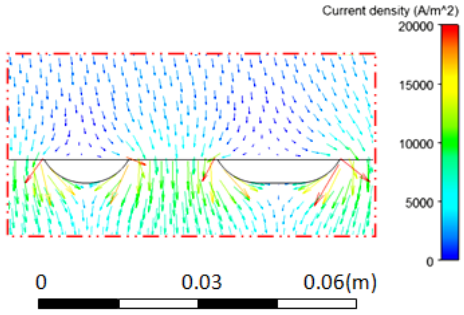

(b)

Figure 8: Current flow with the presence of the bubble layer: (a) full simulation domain; (b) a close-up view near the anode-bath interface.

CONCLUSION

Bubble induced electrical resistance in the Hall-Héroult process has been numerically investigated using a two-dimensional geometry representative of part of an aluminium cell. The main findings from this study are:

- The predicted voltage drop due to bubbles is approximately 0.11 V for a bubble coverage of 37% and 0.29 V for a bubble coverage of 50% when the current density is set 0.7 A cm^{-2}. These values are in reasonably agreement with the experimental measurement.
- The predicted bubble induced resistances are within the range of published empirical correlations, but does not fit in any particular expression. The predicted increasing in the rate of resistance as a function of the bubble coverage is higher than given by empirical predictions.
- The presence of bubbles does not greatly affect the global current flow in the whole cell, but it does significantly affect the local current flow at the anode bath interface. Local peaks in current flow occur at the bubble and liquid boundary on the anode.

Simulation results obtained demonstrate the feasibility of the present modelling approach as an effective numerical tool for the study and prediction of bubble induced electrical resistance. Further numerical modelling studies will be conducted to demonstrate the usefulness of the model for proof-of-concept designs and for practical operations.

REFERENCES

COOKSEY, M.A. TAYLOR, M.P. and CHEN, J.J.J., (2008), "Resistance due to gas bubbles in aluminum reduction cells", *JOM*, **60**, 51-57.

MOLENAAR, D. and DING, K., (2011). "Development of Industrial Benchmark FEA Model to Study Energy Efficient Electrical Connections for Primary Aluminium Smelters", *Light Metals*, 985-990.

FENG, Y.Q., COOKSEY, M. and SCHWARZ, M.P., (2011), "CFD modelling for improvement of alumina feeding system in Aluminium reduction cells", *Light Metals*, 543-548.

EINARSRUD, E.I. and JOHANSEN, S.T, (2011), *8th Int. Conf. on CFD in the Oil, Gas, Metallurgical and Process Ind.*, Trondheim, Norway, June 21-23.

ZHANG, K.Y., FENG, Y.Q., SCHWARZ, M.P., WANG, Z.W. and COOKSEY, M.A., (2012), "Numerical Investigation of Bubble Dynamics in Aluminium Electrolytic Cells", *Light Metals*, 881-886.

DAS, A., MORSI, Y., BROOKS, G., YANG, W. and CHEN, J.J.J., (2011), "The principal characteristics of the detachment and sliding mechanism of gas bubbles under an inclined anode", *10th Australasian Aluminium Smelting Technology Conference*, Launceston, Tasmania, Australia, October 09-14.

EINARSRUD, K. E., (2010), "The Effect of Detaching Bubbles on Aluminum-Cryolite Interfaces: An Experimental and Numerical Investigation", *Metallurgical and Materials Transactions B-Process Metallurgy and Materials Processing Science*, **41**, 560-573.

FORTIN, S., GERHARDT, M. and GESING, A. J., (1984), "Physical modeling of bubble behavior and gas-release from aluminum reduction cell anodes", *Journal of Metals*, **35**, 92-95.

HAUPIN, W., (1971), "A scanning reference electrode for voltage contours in alumium smelting cells", *Journal of Metals*, **23**, 46-49.

GRJOTHEIM, K., Krohn, C. and Thonstad, J., (1982), "Aluminium Electrolysis: Fundamentals of the Hall-Héroult process", 2nd edition (Dusseldorf, Germany: Aluminium Verlag), 146.

CASSAYRE, L., UTIGARD, T. A., and BOUVET, S., (2002), "Visualizing Gas Evolution on Graphite and Oxygen-Evolving Anodes", *JOM*, 41-44.

AABERG, R.J., RANUM, V. and WILLIAMSON, K., (1997), "The gas under anodes in aluminium smelting cells,

Part Π : Gas volume and bubble layer characteristics", *Light Metals*, 341-346.

MAXWELL, J.C., (1954), "A Treatise on Electricity and Magnetism",Unabridged 3rd ed. (NY: Dover Pub).

SIDES, P. J. and TOBIAS, C.W., (1980), "Primary potential and current distribution around a bubble on an electrode", *Journal of the Electrochemical Society*, 288-291.

SOLHEIM. A. and THONSTAD, J.,(1986) "Model cell studies of gas induced resistance in Hall-Heroult cells", Light Metals, 397-340.

THONSTAD, J., (2001), " Aluminium Electrolysis: Fundamentals of the Hall–Héroult Process",3rd ed. (Dusseldorf:Aluminium-Verlag), 115 – 120.

ACKNOWLEDGEMENT

The work is financially supported by CSIRO Mineral Down Under Flagship. Kaiyu Zhang thanks the China Scholarship Council (CSC) for a visiting PhD scholarship and the China Nature Science Foundation Grant under grant No: 51228401.

